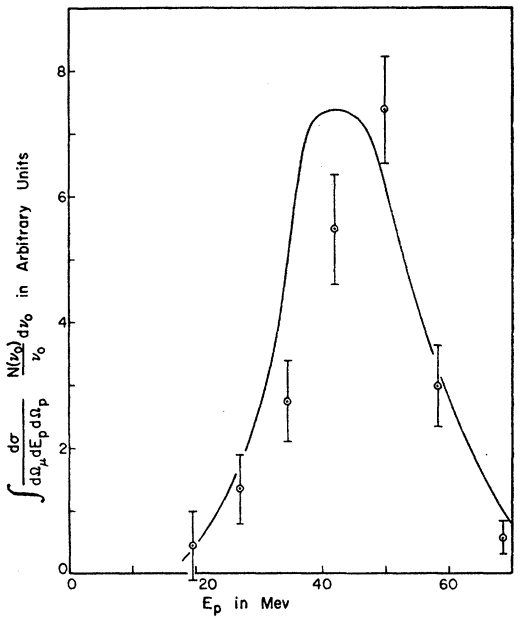

FIG. 1. Energy distribution of protons at 30° in coincidence with 56±9-Mev mesons at 90° produced by 310-Mev bremsstrahlung. The experimental points are those of Keck and Littauer. Normalization is to equal maximum ordinates.

$+\mathbf{D}/2$ is the nucleon's laboratory momentum composed of internal and center-of-mass momentum. $\mathbf{P}$ and $\mathbf{D}$ make angles θ_p and θ_D, respectively, with $\mathbf{v}$. Using these relations the easily derived $d\sigma/d\Omega_\mu d\mathbf{k}_f$ is transformed to

$$\frac{d\sigma}{d\Omega_\mu dE_p d\Omega_p}=\frac{MP\mu\mu_0[\mu(\mu_0+2M)-\mu_0\nu_0\cos\theta_\mu]}{32\pi^2|\mu(\mu_0+M)+\mu_0 P\cos(\theta_p+\theta_\mu)-\mu_0\nu_0\cos\theta_\mu|}\mathfrak{F}, \quad (1)$$

where $E_p=P^2/2M$, and $\mathfrak{F}$ is $(K^2+L^2)[|O_f|^2+\frac{1}{3}(|E_f|^2-|O_f|^2)\times\cos^2\gamma]$ for $\pi^\pm$, and $(K_n{}^2+L_n{}^2+K_p{}^2+L_p{}^2)[\frac{1}{3}(|O_f|^2+|E_f|^2)+(|E_f|^2-|O_f|^2)\cos\delta]$ for π^0, with $\cos^2\gamma=K^2/(K^2+L^2)$ and $\cos\delta=\mathrm{Re}(\frac{1}{3}\mathbf{K}_n{}^*\cdot\mathbf{K}_p+L_n{}^*L_p)/(K_n{}^2+L_n{}^2+K_p{}^2+L_p{}^2)$.

One possible application is the nucleon's energy spectrum for sharply defined θ_p and θ_μ. For free nucleons these two variables determine a $\bar{\mu}_0$ and $\bar{E}_p$. In coincidence with the deuteron's mesons in a range $\Delta\mu_0$ at $\bar{\mu}_0$ one expects nucleons with energies distributed about a peak at $\bar{E}_p$. Multiplication of the above by $d\nu_0 N(\nu_0)/\nu_0$ and integration over $\nu_0(\mu_0)$ gives the yield at a particular E_p. The dependence of K^2+L^2 on ν_0 can be had from free nucleon excitation functions. The dominant behavior of the above is given by $|E_f|^2$ and $|O_f|^2$, which are, when one uses plane waves to describe the final two-nucleon system,

$$\frac{\alpha(\beta^2-\alpha^2)^2}{2\pi^2(1-\alpha\rho_1)}\left\{\int\frac{1}{(P^2+\alpha^2)(P^2+\beta^2)}\pm\frac{1}{(P^2+\alpha^2-2\mathbf{k}_f\cdot\mathbf{D})(P^2+\beta^2-2\mathbf{k}_f\cdot\mathbf{D})}\right\}^2, \quad (2)$$

the upper and lower signs for $|E_f|^2$ and $|O_f|^2$, respectively. These peak at $\bar{E}_p$, $\bar{\mu}_0$. For the particular case of Fig. 1 the plane wave approximation is quite good, but results are insensitive to γ. Correction for the finite experimental $\Delta\theta_p$ and $\Delta\theta_\mu$ widens the theoretical curve by several Mev at half-maximum, but does not affect the location of the maximum. Thus both the half-width and the location of the maximum are at variance with experiment. This is not understood, although a number of suggestions have been investigated. The theory already includes a 3-Mev shift of the peak to higher energies due to the deuteron's binding energy.

The effect on photomeson production of a model suggested by various authors, particularly Wilson,[3] has also been investigated. If mesons are produced while the nucleons are within a meson Compton wavelength of each other, which is about $\frac{1}{5}$ of the time, then reabsorption and photodisintegration are assumed to result. In this model one then expects photomeson production cross sections roughly 20 percent below the Chew and Lewis value. The above energy widths are likewise different in this model. At present statistics on the deuterium to hydrogen ratios are not good enough to either establish or refute this model.

The author is indebted to Professor H. A. Bethe for his encouragement and to Mr. M. E. Miles for doing the numerical calculations.

* AEC Postdoctoral Fellow.

[1] G. F. Chew and H. W. Lewis, Phys. Rev. **84**, 779 (1951). The notation of these authors is used throughout ($c=\hbar=$meson mass $=1$).
[2] J. Keck and R. Littauer, Phys. Rev. **88**, 139 (1952).
[3] R. R. Wilson, Phys. Rev. **86**, 125 (1952).

Domain Properties in $BaTiO_3$

WALTER J. MERZ
Bell Telephone Laboratories, Murray Hill, New Jersey
(Received August 21, 1952)

WE have investigated the arrangements and movements of the ferroelectric domains with an electric field in very good single crystals of $BaTiO_3$. The behavior has been studied both in so-called *a* plates, where the polar axis lies in the plane of the plate, and in *c* plates, where it is perpendicular.

Published descriptions of domains in $BaTiO_3$ have heretofore reported only so-called 90° walls, i.e., those between domains having their polar axes perpendicular to each other. It has usually been assumed that domains polarized antiparallel must also be present, so that each region heretofore called a domain is made up of many smaller antiparallel regions which are the true domains. These 180° walls have now been observed and studied in our work.

Domain boundaries in $BaTiO_3$ crystals are observable, owing to strain birefringence and changes in the refractive index. The strains are larger around a 90° wall than around a 180° wall which makes the 90° wall much sharper and more pronounced. However, the 180° walls can also be seen more easily if one applies an electric dc field perpendicular to the antiparallel domains. The field turns the polar axis of the antiparallel domains a little in opposite directions which increases the internal strain and also shifts the extinction position by a small angle in opposite directions. The antiparallel domains are shown in Fig. 1 by the light and dark lines, for example, at *A*.

Another evidence of the 180° walls is shown in crystals where the antiparallel domains cross 90° walls, which are in this case

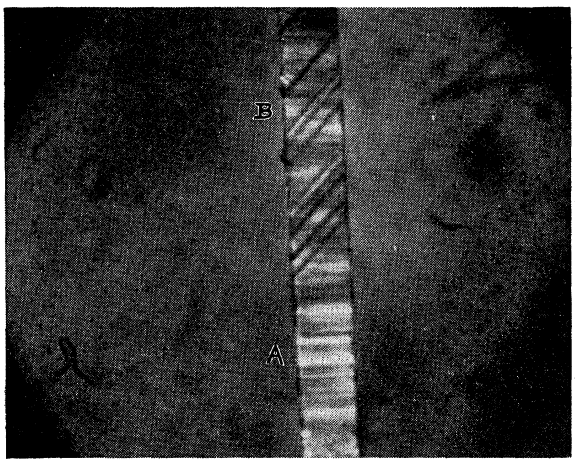

FIG. 1. Edge of a *c* crystal. Total width of crystal $=4\times10^{-3}$ cm.

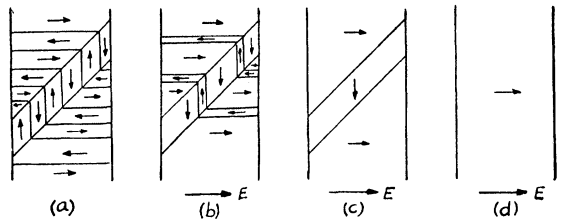

FIG. 2. Schematic arrangements of domains as in Fig. 1 when a field is applied. Observe the head-to-tail arrangement.

at about 45° to the a and c directions. We then can see sharp zigzag lines as in B of Fig. 1. This is shown schematically in Fig. 2(a). If a field is applied in the $+c$ direction, one can move the whole zig-zag line until everything is polarized parallel to the $+c$ direction except the 45° band itself as in Fig. 2(c). At higher field strengths this band also disappears [Fig. 2(d)].

The average width of the antiparallel domains as measured by microscope is from 10^{-5} cm. to about 10^{-3} cm. Whether the width depends on the length of the domain cannot be decided yet.

The observation of antiparallel domains by looking at the edge of a c crystal when an electric field is applied in the c direction was made simultaneously with the observation of the hysteresis loop. Going through the cycle very slowly (using a dc amplifier), we could compare every step of the hysteresis loop with the corresponding domain movements. The loop obtained for the best crystals is shown in Fig. 3.

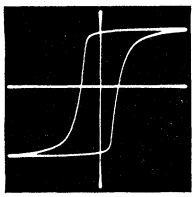

FIG. 3. Hysteresis loop of $BaTiO_3$.

In contrast to the behavior of domain walls in ferromagnetics, it seems to be energetically easier to create new domains than to make an existing properly polarized domain grow larger. We observe hundreds of small new domains which appear very suddenly when a field is applied, thus causing the "low field corner" of the hysteresis loop to be sharp. When more than about half of the domains point in the direction of the applied field, a further increase in the field causes the remaining oppositely orientated domains to change orientation. This wall motion process goes more slowly and requires higher field strengths. This difference can be seen optically as well as in the fact that the "high field corner" of the loop is round.

More detailed studies of the number of domains, their velocities and relaxation times are being carried out by applying very short square electrical pulses. We are especially interested in the dependence of the domain motions on length and amplitude of the applied pulses and the changes with temperature.

I would like to thank Dr. P. W. Anderson and Dr. J. K. Galt for many helpful discussions and Mr. J. Remeika for the preparaof the very good crystals.

Scintillators and Energy Transfer Processes

C. REID
Department of Chemistry, University of British Columbia, Vancouver, Canada
(Received September 3, 1952)

KALLMANN and Furst[1-3] have investigated the relative efficiencies as scintillation counters for γ-rays and α-particles of various organic molecules in solution. The phenomena occurring in such systems are briefly summarized in Fig. 1. For an efficient scintillation process (e) the requirements are obviously: (a) high efficiency of solvent-solvent transfer of electronic energy (i) relative to radiationless quenching in the solvent, so that energy transport from the body of the solvent to a solvent molecule adjacent to the dissolved molecule is possible; (b) high probability of transfer from the solvent to an adjacent solute molecule (t), but low efficiency of the reverse process; (c) high probability of emission from the excited solute molecule (e) relative to self- (c), or solvent (s), quenching.

The conditions necessary to fulfill these processes will be dealt with separately.

1. Solvent-solvent transfer. It has been pointed out elsewhere[4] that efficient energy transfer between identical molecules will occur only if the transfer process is rapid compared with the rate of loss of vibrational energy in the excited electronic state, since otherwise the remaining electronic energy (b in Fig. 2) is insufficient to excite a second molecule, which process requires energy a. Accordingly, we expect good solvents to be those with high polarizability (good electronic coupling with adjacent molecules) but with few branches or long side chains which would facilitate dissipation of vibrational energy. An examination of the solvents most efficient in liquid scintillator systems (xylene, toluene, aniline, benzene, etc.) show that they are, in fact, usually polarizible aromatic molecules of this kind. Any substituents present are of the electron donating kind which further increase the π-electron density of the aromatic ring and thus the polarizibility.

2. Solvent-solute transfer. High efficiency at the solvent-solute transfer step is dependent on good electronic coupling between the two kinds of molecules, but retransfer back to the solvent must be prevented by rapid loss of excited state vibrational energy by the solute. This can be best attained if the molecule is of a "flapping" kind with low vibrational frequencies. Thus we find the most efficient solution scintillators often among this kind of molecule (terphenyl, diphenyl hexatriene, phenyl-α-naphthylamine, etc.). For such molecules both retransfer to the solvent and "self-transfer" (st) to other dissolved molecules is minimized.

3. Emission of radiation. The last-mentioned process, self-transfer between solute molecules, results in a decreased emission probability per unit time and consequently increases the chance of energy loss by competing radiationless processes. Condition (3), like (2), is therefore best met by solutes for which the loss of upper state vibrational energy is rapid.

It has already been shown experimentally[4] that some aromatic substances show self-transfer in solid solutions in inert solvents at low temperature, whereas others do not. Clearly, molecules

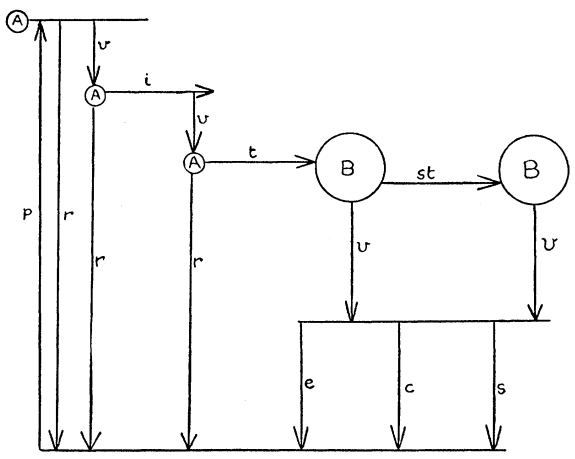

FIG. 1. Steps involved in liquid scintillation. A = solvent molecule energy levels; B = solute molecule energy levels; p = primary excitation of solvent by γ-ray; r = nonradiative solvent quenching; v = loss of vibrational energy (this step may include radiationless crossover to lower electronic levels of the same molecule); t = solvent-solute transfer process; st = self-transfer in solute; e = light emission; c = self-quenching; s = solvent quenching.

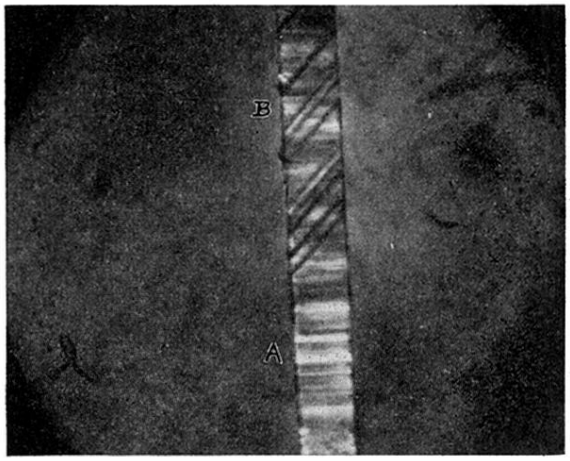

FIG. 1. Edge of a c crystal. Total width of crystal $=4\times10^{-3}$ cm.